RADIO EMISSIONS FROM FILAMENTARY SOURCES: A SIMPLE APPROACH

P. Louarn*

Abstract

A simple study of a new model of the generation of the non-thermal radio emissions - the filamentary source model - is proposed. At variance with most of the models proposed so far, this model, directly suggested by observations made in the terrestrial magnetosphere, takes into account the small scale geometry of the source regions. It also closely links the particle acceleration and the wave generation. Compared to previous models, it has the advantage to directly explain some of the deep differences between the various types of radio emissions (in the polarisation and spectral characteristics, for example) by only slight modifications of the macroscopic structure of the sources (width of the source, density and energy of the plasma inside the source, density variation between the source and the external plasma, etc.) and not by intrinsically different generation processes. It could thus offer a relatively simple interpretation of the complexity of the coherent radio emissions of planetary and, possibly, solar and stellar origins.

1 Introduction

In classical models of the generation of the planetary radio emissions, no particular assumption is made on the small scale structure of the source regions (at the exception of the works of: [Calvert, 1981a; Pritchett, 1986; Pritchett and Winglee, 1989]). This means that one implicitely assumes that the sources are homogeneous at a scale of the order of the wavelength of the emissions. However, in the terrestrial case, one of the important results of the Viking experiment has been to show that this hypothesis of homogeneous sources is not valid. It is indeed now well established that the sources of the Auroral Kilometric Radiation (AKR, hereafter) are thin filamentary structures, elongated along the magnetic field (B_0), with a typical width of a few kilometers (5 km to 10 km) in a direction perpendicular to B_0 [Bahnsen et al., 1989; Louarn et al., 1990; Ungstrup et al., 1990; Hilgers et al., 1991; 1992; Roux et al., 1993]. These filaments of tenuous energetic plasma (typical density and electron energy of 1 cm^{-3} and a few keV) correspond exactly to the acceleration regions responsible for the precipitation of auroral electrons. Their

*Observatoire Midi-Pyrénées, Toulouse, FRANCE

frontiers with the dense cold external plasma (density of the order of 10 cm^{-3}) are sharp density gradients with a typical scale of a few 100 m. Given the particular geometry of the source regions, we call this model suggested by the Viking measurements, the filamentary source model.

As sketched in Figure 1, this model is based on the idea of a structuration of the auroral plasma due to localized acceleration processes. The physics of the auroral acceleration is still largely unknown, nevertheless, a converging set of observations (for example using the data of the FREJA spacecraft: [Louarn et al., 1994; Wahlund et al., 1994; Volwerk et al., 1996]) indicates that the auroral particle acceleration is likely linked to the dissipation of the Poynting flux of Alfven waves and takes place in regions having a typical scale of a few kilometers perpendicular to B_0. The dissipation of energy in the auroral regions could thus create filamentary plasma inhomogeneities along the magnetic field that, in circumstances remaining to be understood, become sources of non-thermal radio emissions (see also, Benson and Akasofu, [1984]). This scenario of the AKR generation could be rather general and might be applied for other types of radio emissions. In a more general way, it is indeed likely that the generation of non-thermal radio emissions is intimely associated with the particle acceleration [Kuijpers, 1989] and, since the most efficient acceleration certainly takes place over rather small scales, the filamentary source model would have a rather broad domain of application (giant planets, sun, stars, etc.)

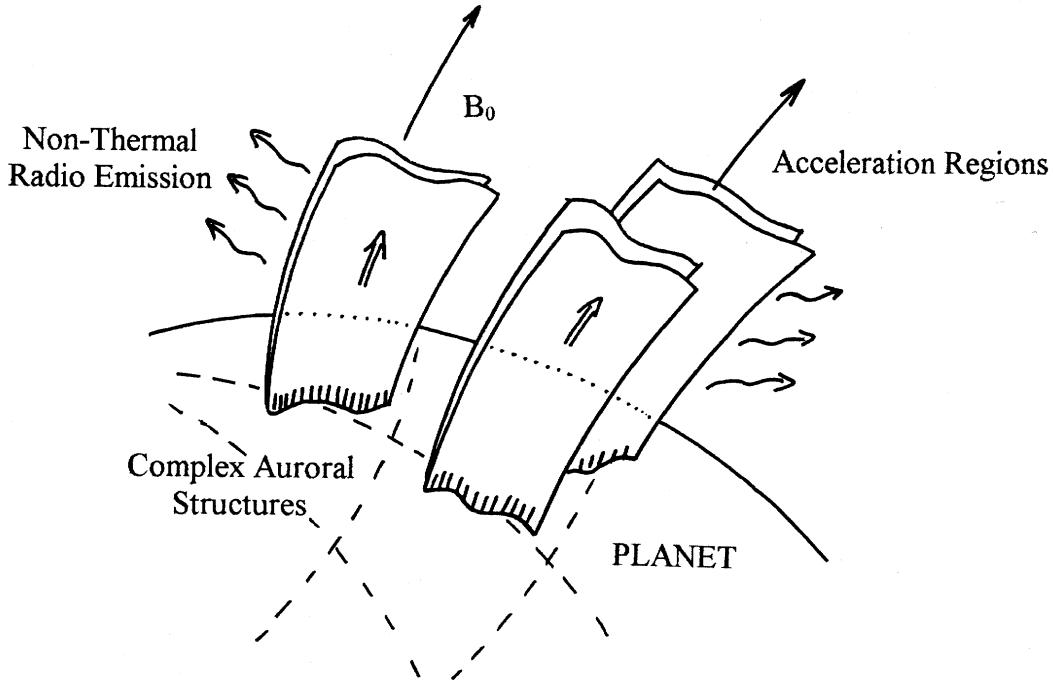

Figure 1: A large scale view of the filamentary source model. The emitting plasma is strongly structured by the acceleration processes. Small scale plasma cavities having a curtain-like or a filamentary geometry are created. They correspond to the sources of the coherent radio emissions.

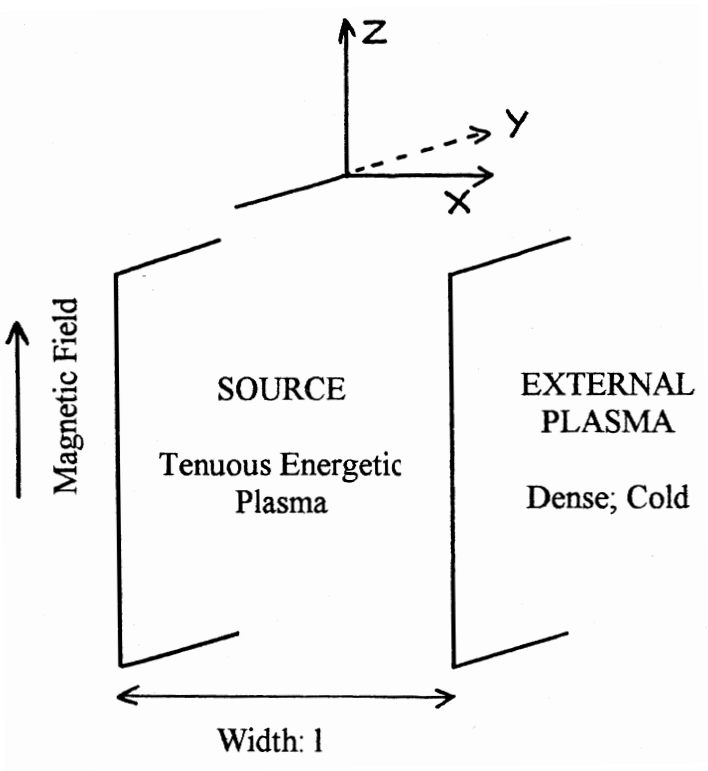

Figure 2: A simple model of the source regions. The typical scale (l) is of the order of a few wavelengths of the emission (a few kilometers for the Earth, 100 m for the decametric jovian emission).

As explained below, the physics of the production of radio emissions by filamentary sources presents important specificities that must be taken into account for the interpretation of the observations. We will not develop and explain here the mathematical formalism that describes the wave generation in filamentary sources. This formalism can be found in two papers [Louarn and Le Quéau, 1996a,b] that will be referenced as paper 1 and paper 2.

2 Radio emissions from plasma cavities

2.1 A simple model of filamentary sources

We will use the model proposed in paper 2. The source has a planar geometry (Figure 2). The external plasma is cold and dense. The plasma of the source is energetic and out-of-equilibrium. It is modelized by an ideal ring-like distribution, a type of distribution adapted to the study of the cyclotron maser instability [Pritchett, 1984; Le Quéau and Louarn, 1989]. Using this idealized model, 5 parameters are sufficient for describing the source: the magnitude of the geomagnetic field, the width of the source (l), the typical electron energy inside the source $< E >$, the internal (n_{int}) and the external (n_{ext}) plasma densities. In the Earth case, the typical values of these parameters are: $B_0 = 9000\,\mathrm{nT}$, $l = 5\,\mathrm{km}$, $< E > = 3\,\mathrm{keV}$, $n_{int} = 1\,\mathrm{cm}^{-3}$, $n_{ext} = 10\,\mathrm{cm}^{-3}$. We will use normalized parameters:

$a = (f_p/f_c)^2$ for the internal plasma
$b = (f_p/f_c)^2$ for the external plasma
$d =< E > /mc^2$: energy of the electrons normalized to the electron rest energy
$L = l\, f_c/c$: width of the source normalized to the wavelength of the radiation in vacuum.

They have the following typical values (in the terrestrial case):
$a \sim 0.4 \cdot 10^{-2}$, $b \sim 2 \cdot 10^{-2}$, $d \sim 10^{-2}$, $L = 15$

As seen later, the scale of variation of the geomagnetic field is another important parameter. For a dipolar field and making a linear approximation: one has $B(z) \sim B_0(1 - z/H)$; with $H = R/3$ where R is the distance to the center of the planet.

2.2 Wave dispersion inside and outside the sources

In paper 2, a simplified dispersion equation has been obtained for describing the wave propagation at frequencies close to the gyrofrequency for both cold and relativistic plamas. The associated dispersion curves are presented in Figure 3, for a range of parameters adapted to the generation of planetary radio emissions. As we are only interested by the wave propagation at frequencies close to f_c, we use a normalized frequency: $Z = (f - f_c)/f_c$. Using this variable, the cut-off frequency of the X mode in the external plasma is thus simply: $Z_{cut} = b$. We will distinguish the modes that propagate inside the source and outside the source by calling them: internal and external (X, O or Z) modes.

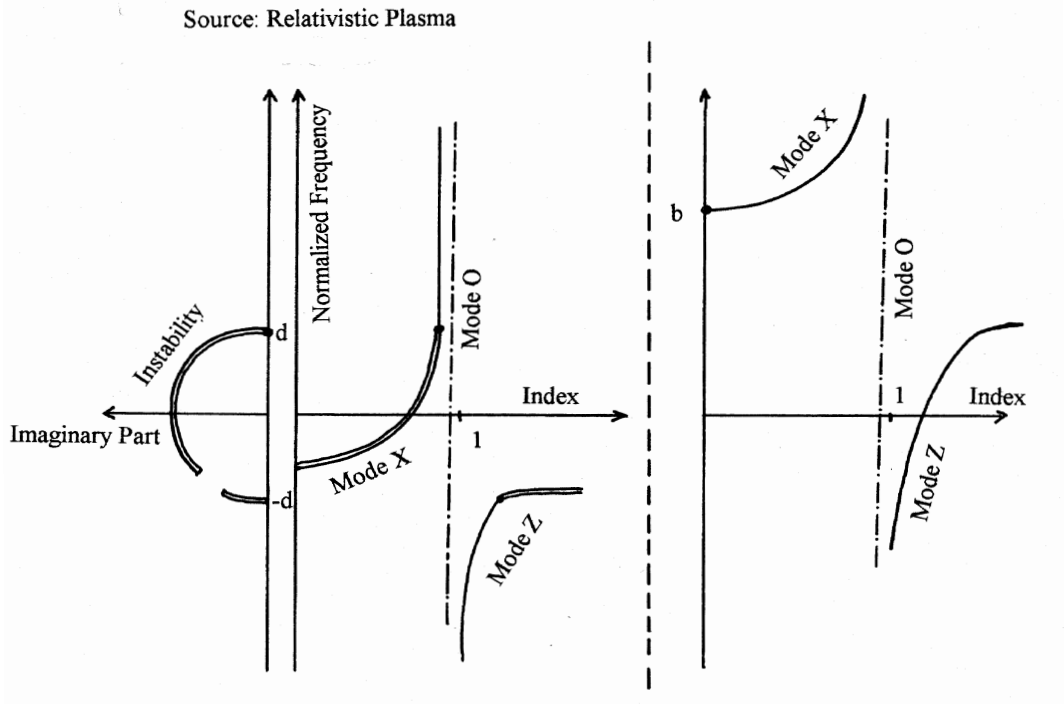

Figure 3: Dispersion curves at frequencies close to f_c, in relativistic plasma (left panel) and in the classical cold plasma case (right panel).

As seen in Figure 3, an instability exists in the relativistic plasma. The most unstable waves propagate perpendicularly, on the X mode, at $Z \sim 0$ ($f \sim f_c$), the normalized growth rate being of the order of d. The maser mechanism is thus expected to create the initial electromagnetic energy on the internal X mode, the maximum wave intensity being at frequencies close to f_c. These dispersion curves correspond to the propagation in an homogeneous plasma. If the finite geometry effects are taken into account (see paper 2), the exact calculation shows that the domain of instability is significantly below f_c. This shift of the instability domain below f_c depends on the energy and on the width of the source. For typical source width ($L = 10 - 20$), the maximum instability is at normalized frequencies close to $Z = -d/2$.

For the filamentary source model, the production of the radio emission results from the transfer of the electromagnetic energy generated inside the source into modes that propagate in the external plasma. This mechanism is studied by investigating how the internal unstable waves can be connected to the external modes. One sees immediately the potential difficulty of producing an X mode emission. Indeed, in the external plasma, only the O and the Z modes exist in the unstable frequency domain. There is then no possibility of direct connexion between the internal unstable waves and the external X mode.

The analysis of the dynamic spectra measured by Viking during the crossing of AKR sources helps to understand the mechanism of production of the X mode radio emission (see paper 1 and Figure 4-a). Inside the source, the maximum wave intensity is on the X mode at frequencies very close to the gyrofrequency, which is consistent with a wave generation due to the maser cyclotron instability. The intensity then decreases as the frequency increases. In the external plasma, two frequency domains have to be considered. From the frequency of generation to a frequency a few percents above the external X mode cut-off, the emission is dominated by the O mode. This shows that a filamentary source can produce a certain amount of O mode by a mode conversion of the internal unstable X mode. The O mode intensity is however much lower (at least 20 db) than the wave intensity measured inside the source. Above this frequency domain, the X mode component of the emission is dominant. Its level is comparable to the level of the internal waves, suggesting that the internal X mode/external X mode transmission coefficient is close to 1.

A simple explanation of these observations would be the following (see paper 1 and Figure 4-b): After its generation on the internal X mode at frequencies close to f_c, the electromagnetic energy propagates upwards, towards regions of decreasing magnetic field. Due to this upward propagation, the waves reach altitudes of lower X mode cut-off. Then, above a certain altitude, the external X mode cut-off becomes smaller than the frequency of the waves and the connection with the external X mode becomes possible. During the upward propagation, the internal waves are connected to the O and the Z external modes and a part of the initial energy is thus converted into external Z and O modes. Nevertheless, the transmission coefficients (internal X mode $\rightarrow$ external O or Z modes) being small; the electromagnetic energy remains thus relatively confined inside the source until the connexion with the external X mode becomes possible.

This indirect production of the observable radio emission by a mode conversion at the source frontiers is one of the specificities of the filamentary source model. As discussed

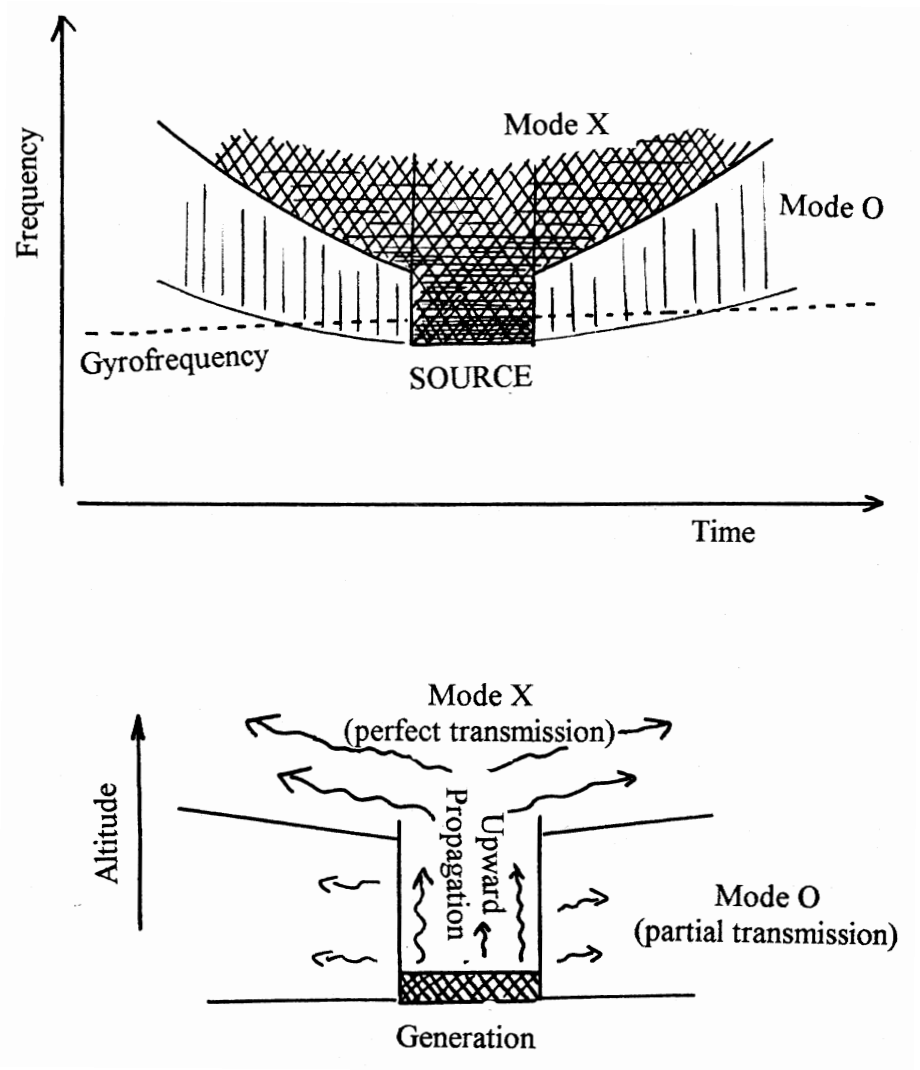

Figure 4: Upper panel (4-a): A sketch on the crossing of an AKR source as seen by Viking. Lower panel (4-b): Propagation of the electromagnetic energy inside the source and the expected mode conversion across the source frontiers.

now, the relative amount of each component (O and X) and, thus the polarisation of the emission, varies with the macroscopic structure of the source.

3 Polarisation of the radio emission generated by filametary sources

The proportion of X and O modes produced by a filamentary source can be evaluated by calculating the different transmission coefficients across the source frontiers. They will be noted T_{xo}, T_{xz} and T_{xx} for the transmission from the internal X mode to the external O, Z or X modes. The observations show that (1) only very little Z mode is produced and, (2) when the connexion with the external X mode becomes possible, T_{xx} is close to 1. The X/O proportion is thus relatively simple to obtain:

From the region of production of the initial electromagnetic energy to the region of connexion with the external X mode, only T_{xo} has indeed to be considered. The transfer equation inside the source then writes

$$\frac{\partial W}{\partial z} = -2T_{xo}(z)\frac{v_{g\perp}}{v_{g\parallel}}\frac{1}{L}W \tag{1}$$

with:
$v_{g\perp,(\parallel)}$: perpendicular and parallel group velocity
L: width of the source
W: electromagnetic energy

This equation has to be integrated from the altitude of production of the energy ($z = 0$) to the altitude of connexion with the external X mode ($z = h$). The nearly perfect transmission T_{xx} guarantees that the energy not converted into the O mode during the upward propagation from $z = 0$ to $z = h$ will escape the source on the X mode. The quantity of X mode produced by a source is:

$$W(h) = W_0 \exp\left[-2\int_0^h T_{xo}\frac{v_{g\perp}}{v_{g\parallel}}\frac{dz}{L}\right] \tag{2}$$

The produced quantity of O mode is thus simply: $W_0(1 - A)$.
h is easily evaluated for a linear variation of the magnetic field: $f_c = f_0(1 - z/H)$. Using this linear approximation, the cut-off frequency of the external X mode varies as $f_x = f_c(1+b) = f_0(1-z/H+b)$. As mentioned before, $Z = -d/2$ is the typical normalized frequency of the waves generated at $z = 0$. These waves can connect with the external X mode when $f > f_x$ or, using normalized variables, when $Z = -d/2 > b - z/H$ and consequently, $h = H(b + d/2)$. In the terrestrial case ($H = 15000$ km and $b \sim d \sim 10^{-2}$), h is of the order of 200 km. The typical upward propagation of the waves needed before their escape out of the sources is thus of a few 100 km.

The calculation of the transmission coefficients is straightforward using the continuity equations of the components of the electromagnetic field [Jackson, 1962, p. 276]. As this will be presented into details elsewhere, the parametric study shows that T_{xo} is approximately given by:

$T_{xo} \sim 10^{-5}\, b\, d^3$

Integrating Equation (1) from $z = 0$ to $h = (b + d/2)H$, one thus obtains the relative proportion of X and O mode produced by a source:

$\mathrm{O/X} \approx (1 - A)/A \quad \text{with} \quad A \approx \exp\left[-10^{-4}\, b\, d^3\, (b + \frac{d}{2})\, H/L\right]$

This simple expression describes the main properties of the polarisation state of the emission. It shows that the proportion of O mode increases if:
- the energy of the emitting particles increases (role of d)
- the density of the external plasma increases (role of b)
- the distance from the planet increases (role of H)
- the width of the sources decreases (role of l)

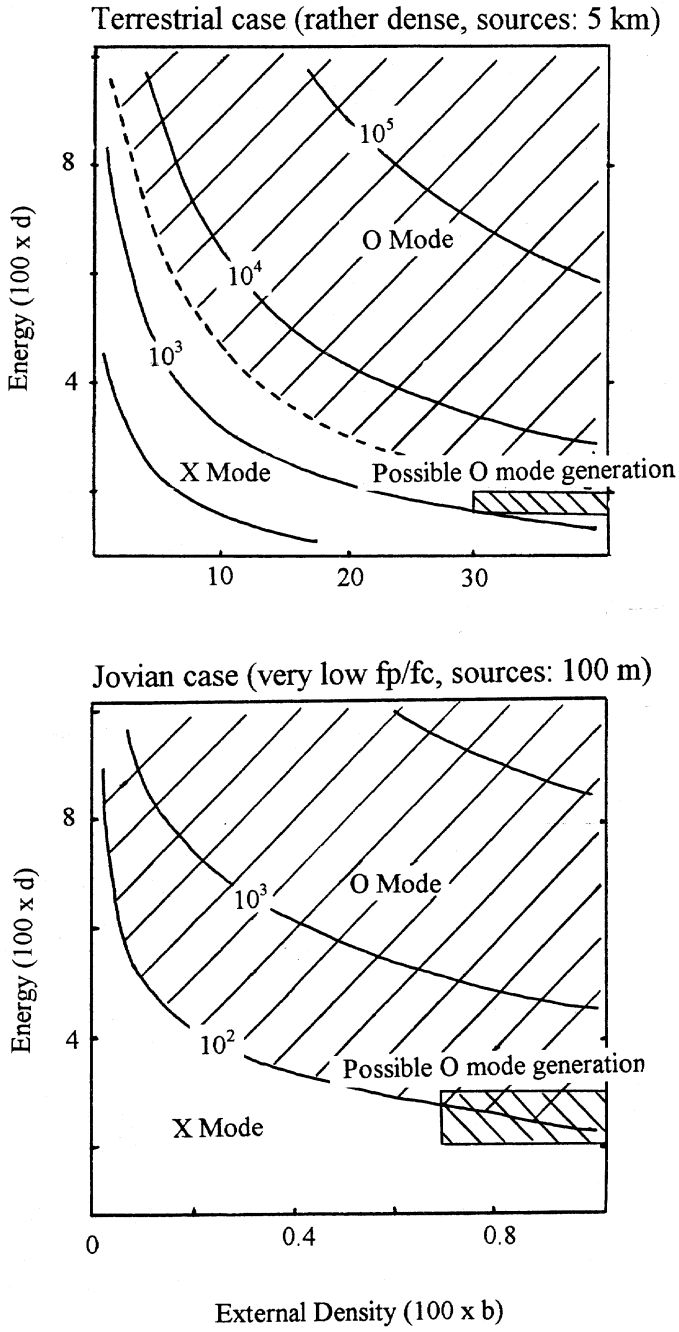

Figure 5: Polarisation of the radiation of a filamentary source as a function of the energy (d) and of the density in the external plasma (b). These two parameters are here multiplied by 100; $d = 4$ on the vertical scale corresponds to 20 keV electrons. The widths of the sources are in meters.

In conclusion, narrow energetic sources, embedded in a dense plasma, will produce an O mode emission.To illustrate these results, we present in Figure 5 two parametric studies corresponding to the terrestrial and the Jovian cases. For two distances from the center of the planet (15000 km for the Earth and 70000 km for Jupiter) and for different

widths of the sources, the domains of dominant X or O mode emissions are shown in the energy/density plane (b, d plane). For the terrestrial case, one sees that only relatively extreme conditions (width smaller than 5 km, strong density: $b \sim 0.3$ and high energy: 10 keV) lead to the generation of a large proportion of O mode. This is consistent with the Viking observations. Indeed, only the most energetic source crossed by Viking, which is also relatively narrow and in a dense plasma (the source crossed during the orbit 176, see paper 1), emits a dominant O mode component. In the other cases, the X mode is always dominant. For the Jovian case, the expected very low values of b due to the strong magnetization of the plasma makes the O mode production more difficult. Even for very narrow sources and energetic particles, the X mode is thus expected to dominate. It is nevertheless possible that energetic sources, at low altitudes (so that b is a little larger), emit O mode waves.

One of the important characteristics of the filamentary source model is thus to separate the initial generation of the electromagnetic energy (the maser inside the source) and the production of the observable radio emission (conversion across the source frontiers). The present discussion could be extended to other types of radio emissions. For example, in the solar corona, there is no physical principle that forbids the use of the filamentary source models. During a flare, the global energy release could well take place over small scale regions that could be also the sources of non thermal emissions. This leads to the hypothesis of a highly structured fibrous-like corona presenting strong small scale plasma inhomogeneities. In such a situation, the different observed polarisations would simply result from the conversion processes at the frontiers of the sources and no specific generation process would thus be needed for explaining these differences.

4 The radiating diagram of filamentary sources

The classical maser cyclotron theory predicts that the radiating diagram of a source is a largely open hollow cone with a cylindrical symmetry around the magnetic field. In the present case, the filamentary geometry creates an asymmetry around the magnetic field, a new situation that deserves some comments.

The radiating diagram of a filamentary source can be described by considering some simple properties of the wave generation and propagation in regions of finite geometry (see paper 2 and Figure 6):
(1) The maser mechanism is especially efficient for waves propagating perpendicularly to the magnetic field, with refractive index close to 1. The x and y directions are however not equivalent: k_y is a free parameter and k_x is quantified. The unstable waves have thus preferential directions of propagation (Figure 6, lower left). The initial radiating diagram is thus a succession of narrow beams in the plane perpendicular to B_0.
(2) During their propagation inside the source, the waves are progressively refracted upwards. This refraction being more important for waves having a small index, the initial radiating diagram is modified as shown in Figure 6, upper left. Waves with small k_y acquire a relatively strong k_z when waves with high k_y remain in a quasi perpendicular direction.
(3) The radiating diagram is further modified at the crossing of the source frontiers. T_{xx}

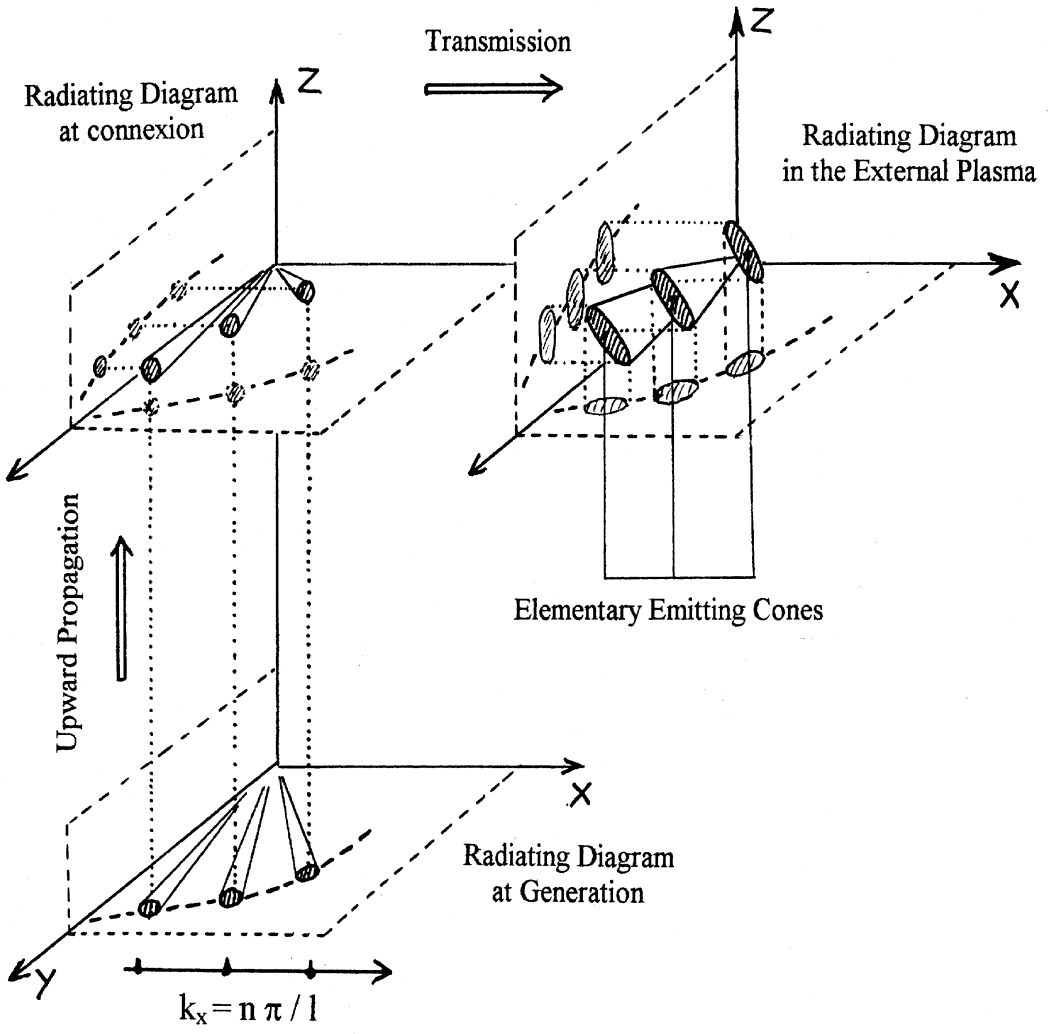

Figure 6: Radiating diagram of a source. Lower left: at the generation (strictly perpendicular propagation); Upper left: inside the source, just before the connexion with the external X mode; Upper right: in the external plasma, after connexion.

indeed sharply varies near the altitude of connexion. It goes from 0 to 1 over a small altitude range which also corresponds to a rapid rotation of the k vector. The result is an opening and a broadening of each of the elementary cones of emission. The final geometry of the radiating diagram is thus relatively complex (Figure 6, upper right). It is a juxtaposition of different narrow emitting cones with axis more parallel to B_0 when the angle with the tangent to the source increases. The aperture of each of the elementary cones is a fraction of degrees. Their angular separation, linked to the k_x quantification, depends on the width of the source. It is typical of the order of 5 for $L = 10 - 20$. Let us also note that waves remaining the longest time in the source are more amplified by the maser mechanism. The y direction (direction of invariance of the source) is then a preferential direction of emission. The different elementary cones are thus certainly not equivalent. The one with the closest to y direction corresponds to waves that have optimized their amplification path and dominate.

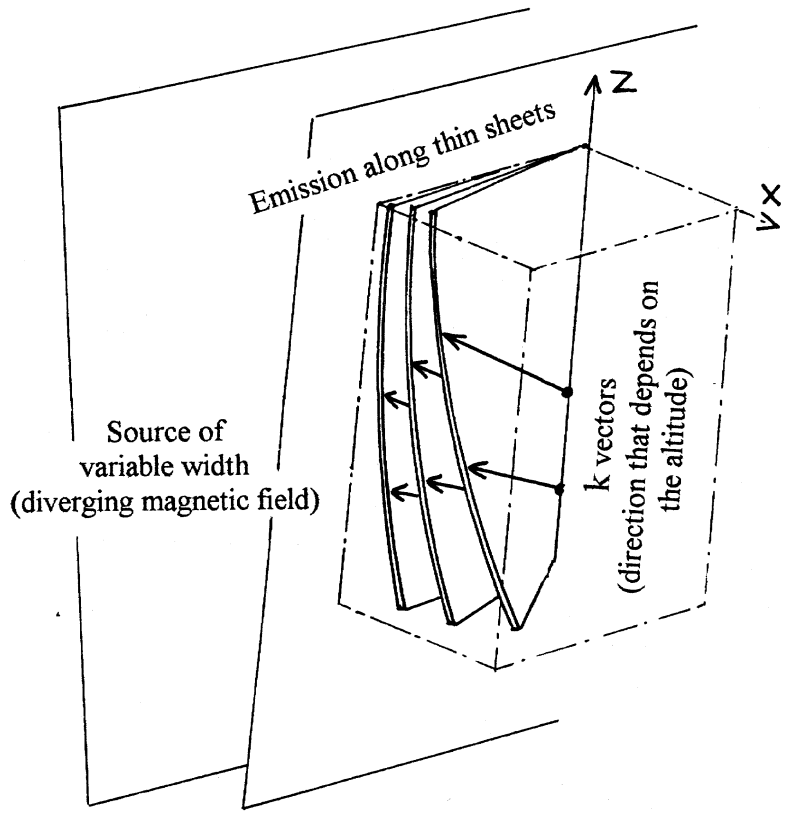

Figure 7: The complete radiating diagram of a source. The emission propagates along thin sheets making a variable angle with respect to the source.

Figure 6 corresponds to the radiating diagram observed at a given altitude. The extension of the source along the magnetic field must also be considered. Since the magnetic field and the width of the source vary with the altitude, the values of k_x selected by the condition of quantification also depend on the altitude. The source being narrower at low altitudes, the radiating diagram is more open for sources closer to the planet (Figure 7). Depending on the orientation of the observer with respect to the source, waves of different frequencies will be then detected. This can be used for understanding how a filamentary source could generate emissions presenting a great variety of spectral fine structures.

5 The filamentary source model: An explication of the spectral complexity of the radio emissions?

As mentioned in the introduction, the sources of the AKR are closely associated with the acceleration regions responsible for the precipitation of the auroral electrons. It can thus be hypothesized that the visual discrete auroral forms give an image of the morphology of the sources of non-thermal radio emissions. This would mean that the sources, organized in curtain-like structures, present an extreme diversity of morphologies and of dynamical behaviours. What would be the radio emissions detected by a distant observer in such situations?

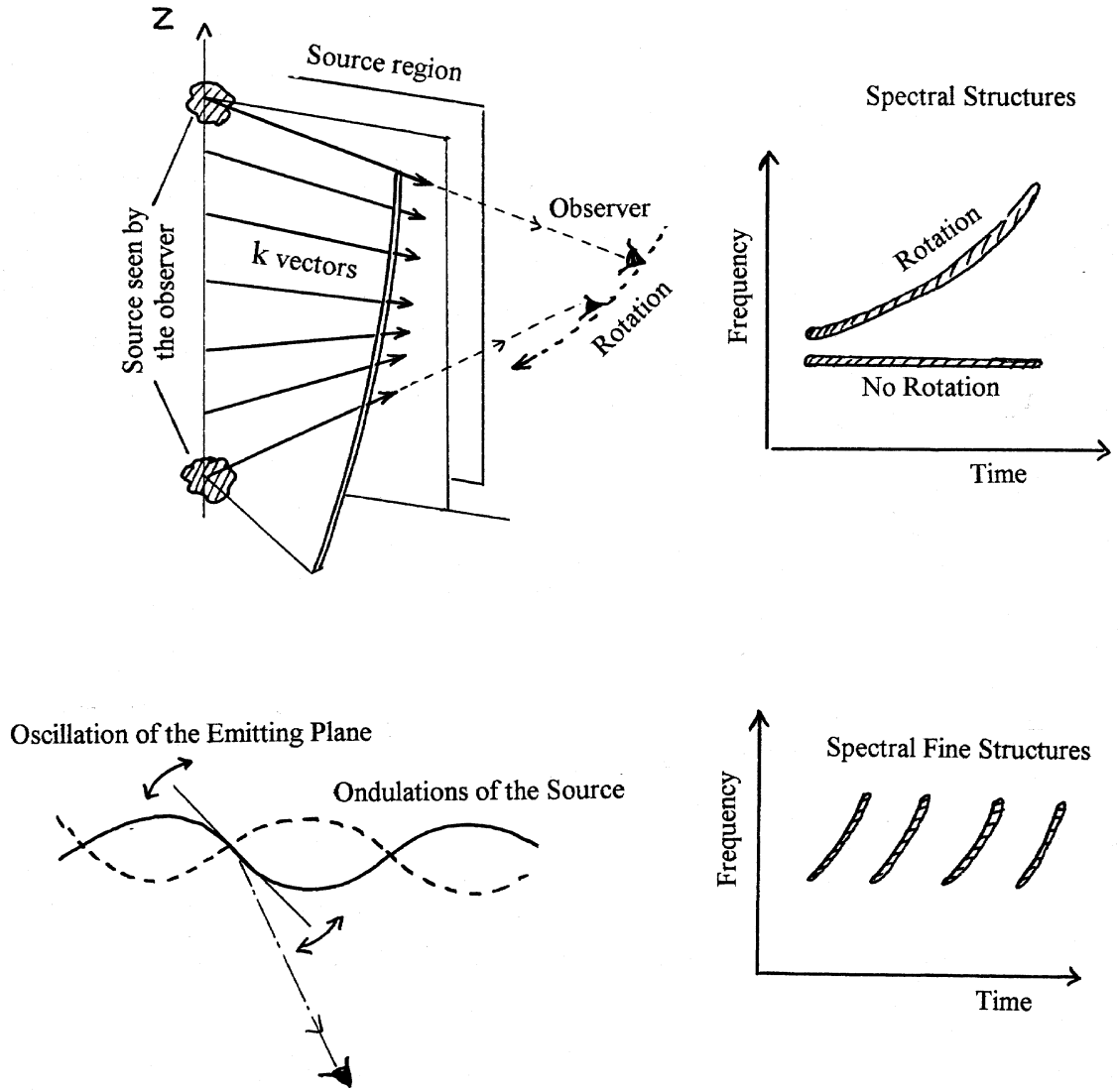

Figure 8: A simple model for explaining the complexity of the spectral fine structures of some radio emissions.

In most cases, the complexity is so high that the radiating diagrams of each portions of the sources are just mixed. This is likely the case of the AKR, during periods of intense auroral activity, when a large fraction of the auroral zone is covered by discrete auroras. An averaged broadband emission is observed with possibly a few spectral features. However, in other occasions, the auroras present an impressive spatial and temporal organization. As explained in Figure 8, this could create a great variety of spectral structures.

For simplicity, let us assume that the radiating diagram of each portions of the sources is reduced to a unique elementary cone. In the general case, the angle between this elementary cone and the source varies with the altitude. For example, as discussed in the last section, the waves generated at lower altitudes propagate in a more parallel direction than those generated above. Let us first consider a plane structure (case 1). Due to the very directive radiating diagram, the observer sees waves arriving from a well defined

direction and only a restricted portion of the source is visible. The spectral bandwidth of the visible emission is thus relatively small. Now, if the structure moves (for example, if it rotates), the angle α between the line of sight and the source varies. (The angle α is the angle between the line of sight and the plane locally tangent to the source, supposed to be a laminar structure.) Different portions of the sources, from different altitudes, will be visible. The central frequency of the observed radiation is thus modified. For example, it will increase if α increases. Even a rather slow motion of the source could thus result in a short and rapidly drifting radio event.

In order to show the richness of the model, let us study a simple ondulation of the source (case 2). This corresponds to a frequently observed type of motion of discrete arcs. At a given time, for a particular shape of the source, waves coming from a few well defined regions are visible. Due to the ondulations, for each of the visible portions of the source, the angles α vary which leads to a frequency drift of the different spectral components of the visible emission. We suggest that extrapolations of this very simple model could explain the complexity of some radio emissions as, for example, the Jovian S-burst. The basic idea would be to explain this complexity by a spatio-temporal organisation of the sources (see also, Lecacheux et al., [1981]) and not by intrinsic properties of the various microscopic generation processes.